ORIGINAL PAPER

Magnetic-field calculation for a high-temperature superconducting cryogenic current comparator

Vladimir Bubanja

Abstract The problem considered in this paper arises in the design of a high-temperature superconducting cryogenic current comparator (CCC). The CCC consists of two currents flowing in opposite directions inside a toroidal superconducting shield. The shield has a radial cut, necessary for the measurement of the current ratio, but causing an error in the obtained ratio. The problem of interest is the dependence of the error on the geometric parameters of the device: the major and minor radii of the shield, the cut width, the material thickness, and the location of the currents. In the first part of the paper, a toroidal shield with an infinitesimal cut is considered and analytic expressions are derived for the magnetic field and the surface-current distribution. In the second part, a cut of finite width is introduced. Since all the perturbing currents are present in the narrow region around the cut, a shield of cylindrical shape is assumed. Expressions are derived for the flux through the cut and the magnetic field around the cut. Analytical results are in good agreement with the numerical results obtained by a finite-element method. In the final part, the expression for the ratio error is derived, which shows that in order to minimize the error, currents should be concentrated around the shield axis, the major radius of the shield should be maximized and the bore radius minimized. The error depends logarithmically on the cut width.

Keywords Conformal mapping · Green's functions · Superconducting devices

1 Introduction

We consider the magnetic field generated by currents enclosed by a superconducting sheath of both toroidal and cylindrical shape. The problem comes from the design of a cryogenic current comparator (CCC), which as a current amplifying device has unsurpassed accuracy. In precision electrical metrology CCC's are widely used for resistance scaling from the quantum Hall-effect standard [1] and for the amplification of currents generated by single electron-tunneling (SET) devices [2, 3]. They are also used for low dc [4] and ac [5] resistance measurements. A CCC is an integral part of the quantum metrological triangle experiment that is currently under development [6]. The aim of the experiment is to accurately test the consistency of

V. Bubanja (✉)
Industrial Research Limited,
PO Box 31-310, Lower Hutt 6009, New Zealand
e-mail: v.bubanja@irl.cri.nz

the fundamental constants involved in the three quantum effects: Josephson, quantum Hall and SET. In this experiment a CCC is used to amplify the current produced by a quantum current source (the R-pump [7, 8]). This current then passes through the two-dimensional electron gas of a semiconducting device in a high magnetic field, with the transverse Hall voltage being compared to the Josephson-array voltage standard. In combination with the cryogenic capacitor standard [9], the experiment will provide information for the possible future adjustments of the fundamental physical constants involved in the above three effects [10].

In a CCC, two circular wire coils of N_1 and N_2 turns, carry currents I_1 and I_2, respectively, in the opposite direction. The magnetic field at the centre of the coils is sensed by a superconducting quantum interference device (SQUID). For a fixed input current I_1, the current I_2 is adjusted via a feedback system connected to the SQUID, until the ampere-turns of the two currents are balanced. In such a way, the CCC acts as a current transformer, with the output current I_2 being equal to $I_1 N_1 / N_2$ at balance. Ideally, for such system to work, the two wire coils would have to coincide with the same circle, which, owing to the finite thickness of the wires, is not possible. To remove the dependence of the magnetic field (sensed by the SQUID) on the location of the wires, all the windings are enclosed by a superconducting torus. Owing to the Meissner effect, a supercurrent is induced on the inner surface of the torus, with its integral over the inner surface being equal to the ampere-turn imbalance in the windings. If such a torus had an infinitesimal cut in the half-plane containing the rotational axis of symmetry of the torus, this surface supercurrent would, after reaching the cut, flow along the cross-section of the cut and then loop around the outer surface of the torus, allowing the ampere-turn imbalance to be detected by the SQUID (in the absence of the cut no current would flow on the outside surface, and no magnetic field would be sensed by the SQUID). The supercurrent distribution on the inner surface would depend on the mutual inductance between the supercurrent filaments and the windings, which, in turn, is dependent on the winding locations. On the other hand, the supercurrent distribution on the outer surface would be independent of the location of the windings inside the torus.

In practice, however, the cut has small but finite width (a fabricated solid torus is cut, usually by a diamond saw). This exposes the wires to the outside, and therefore the flux measured by the SQUID at the torus centre is affected by the location of the wires. A typical size of the torus is several centimeters in diameter and the cut is about a millimeter. Since a CCC is usually required to have the highest possible accuracy, the effect of the finite cut cannot be neglected. In this paper we derive an analytic expression for the magnetic flux leakage through the cut area, and also an expression for the magnetic field at the SQUID location, both as functions of the geometric parameters of the problem.

In most applications, low-temperature superconducting (LTS) materials, such as lead, are used for shielding. These materials, in the form of a thick foil, can be easily folded in such a form that the torus ends overlap while being electrically insulated. In that way, the effect of the cut can be screened by increasing the overlapping region, so that for large-enough overlap the SQUID detects only the magnetic field of the equilibrium supercurrents flowing on the outside surface of the shield [11]. Aspects of the LTS CCC design have been considered for example in [12] and [13].

Cylindrical shields made of high-temperature superconducting (HTS) materials were considered for noninvasive measurements of the current carried by charged-particle beams [14], and resistance ratio measurements [15]. Such a CCC can be used at liquid Nitrogen temperatures, therefore reducing the cost and complexity associated with using liquid Helium necessary for the operation of a LTS CCC. We consider here a toroidal shield corresponding to the design studied experimentally in [16, 17]. The HTS materials are generally much more difficult to use than the LTS ones. They are brittle and are susceptible to distortion and cracking, making the process of obtaining the desired shape time-consuming. Details of such fabrication, using YBCO powder as the HTS material, are given in [17]. For design purposes it is necessary to have an analytic expression for the ratio error of the CCC as a function of the geometry of the device. That is the goal of our study.

The paper is organized as follows. In Sect. 2, we consider a toroidal shield with infinitesimal cut and derive an analytic expression for the magnetic field inside and outside the torus. In Sect. 3, we introduce a cut of finite width in the shield, and assuming the shield to be cylindrical we find the analytic expressions for the magnetic field and the leakage flux through the cut. In Sect. 4 we obtain the ratio error of the CCC. A summary is presented in Sect. 5.

2 Toroidal shield

We start by considering a closed superconducting torus enclosing a current filament. We make the assumption of ideal diamagnetic behaviour of the superconductor, which is justified in practice, since the typical thickness of the shield is much larger than the London penetration depth. We are interested in deriving an analytic expression for the magnetic field inside the torus. Figure 1 shows the schematic drawing of the device (Note that the cut in the shield is not to scale. In this section the cut is considered to have infinitesimal width. A cut of finite width is treated in the following section).

In the Coulomb gauge, the magnetic vector potential $\mathbf{A}$ satisfies the vector Poisson's equation:

$$\Delta \mathbf{A} = -\mu_0 \mathbf{j}. \tag{1}$$

The natural choice of the coordinate system is the toroidal one (Fig. 2), whose coordinates (η, θ, ψ), with $0 \leq \eta < +\infty$, $-\pi < \theta \leq \pi$, $0 \leq \psi < 2\pi$, are related to the Cartesian coordinates as follows:

$$x = \frac{a \sinh \eta \cos \psi}{\cosh \eta - \cos \theta}, \quad y = \frac{a \sinh \eta \sin \psi}{\cosh \eta - \cos \theta}, \quad z = \frac{a \sin \theta}{\cosh \eta - \cos \theta}, \tag{2}$$

where a is the radius of the toroidal axis (corresponding to $\eta \to \infty$). The coordinate surfaces are toroids for $\eta = \eta_0$ (with major radius $a \coth \eta_0$ and minor radius $a \operatorname{csch} \eta_0$), spherical bowls for $\theta = \pm\theta_0$ (of radius $a \csc \theta_0$ with centers at $\pm a \cot \theta_0$ along the z-axis), and half planes for $\psi = \psi_0$ (bordered by the z-axis, which corresponds to $\eta = 0$). The line element is given by $\mathrm{d}s^2 = g_{ij}\mathrm{d}x^i\mathrm{d}x^j$ with the metric tensor $g_{ij} = \delta_j^i h_i^2$, where δ_j^i is the Kronecker delta, and the scale factors are given by
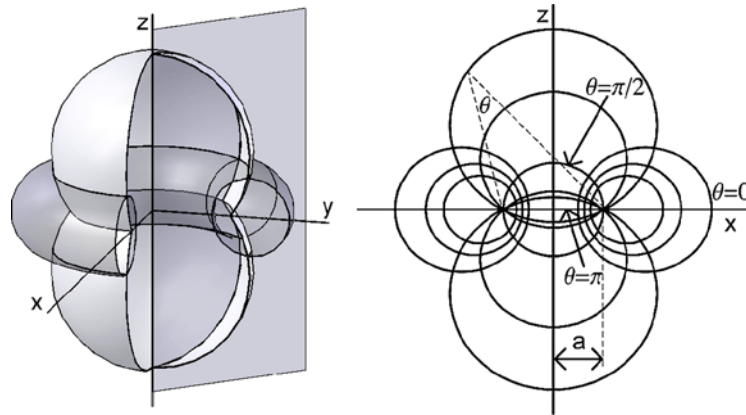
$$h_\eta = h_\theta = \frac{a}{\cosh \eta - \cos \theta}, \quad h_\psi = \frac{a \sinh \eta}{\cosh \eta - \cos \theta}. \tag{3}$$

In order to solve Eq. 1 we will make use of the vector Green's theorem [18, Part II, p. 1768]:

$$\int (\mathbf{E}\Delta \mathbf{F} - \mathbf{F}\Delta \mathbf{E})\mathrm{d}v = \oint \left\{ (\mathbf{E}\nabla \mathbf{F} - \mathbf{F}\nabla \mathbf{E})\hat{\mathbf{n}} - \left[\mathbf{E}(\hat{\mathbf{n}} \times \operatorname{curl} \mathbf{F}) + \operatorname{curl} \mathbf{E}(\hat{\mathbf{n}} \times \mathbf{F}) \right] \right\} \mathrm{d}S, \tag{4}$$

Fig. 1 Toroidal superconductor enclosing a current carrying filament. The filament represents the unbalanced current resulting from the difference of two currents flowing in opposite directions inside the torus
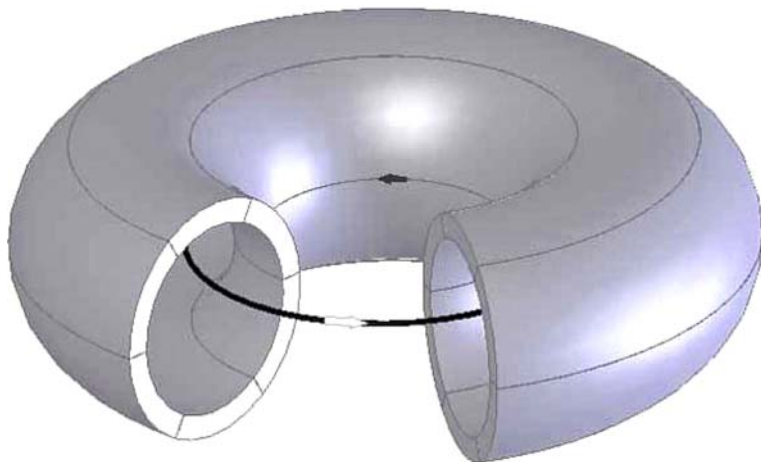
Fig. 2 Toroidal system of coordinates is shown on the left. The cross-section with the half-planes $\psi = 0$ and $\psi = \pi$ gives the bipolar system shown on the right. Using Eq. 2, we may express the relation between toroidal and cylindrical coordinates (r, ψ, z) as $z + \mathrm{i}\, r = a \coth[(\theta - \mathrm{i}\,\eta)/2]$

where the vector Laplacian is given by

$$\Delta \mathbf{E} = \operatorname{grad} \operatorname{div} \mathbf{E} - \operatorname{curl} \operatorname{curl} \mathbf{E}. \tag{5}$$

By using (3) and taking into account the axial symmetry of the generated field, we obtain for the left-hand side of (1):

$$\Delta \mathbf{A} = \hat{\psi} \left[\Delta - \frac{1}{h_\psi^2} \right] A_\psi(\eta, \theta). \tag{6}$$

The magnetic field is generated by the current filament located at $(\eta = \eta_f, \theta = \theta_f)$, so on the right-hand side of Eq. 1 we have

$$\mathbf{j} = \frac{I}{h_\eta h_\theta} \delta(\eta - \eta_f) \delta(\theta - \theta_f) \hat{\psi}. \tag{7}$$

In order to derive the Green's function for the Helmholtz-type equation obtained by substituting (6) and (7) in (1), we start by considering the Green's function for the scalar Poisson equation with the homogeneous Dirichlet boundary condition $G_s = 0$ at $\eta = \eta_0$ (the boundary condition which ensures that the normal component of the magnetic field vanishes at the surface of the superconductor is $A_\psi(\eta_0, \theta) = A_0/h_\psi$ and we can choose the constant $A_0 = 0$):

$$\Delta G_s(\mathbf{r}, \mathbf{r}') = -4\pi \delta(\mathbf{r} - \mathbf{r}'). \tag{8}$$

By using Eq. 2, we can express the inverse distance between two points in toroidal coordinates, which is required for G_s, in terms of the Legendre functions Q_ν, by using the expansion [18, Part II, p. 1304]:

$$\frac{1}{\sqrt{\cosh \eta - \cos \theta}} = \frac{\sqrt{2}}{\pi} \sum_{n=0}^{\infty} \epsilon_n Q_{n-\frac{1}{2}}(\cosh \eta) \cos(n\theta), \tag{9}$$

where $\epsilon_n = 2 - \delta_n^0$ is the Neumann factor. Legendre functions can be expressed in terms of the associated Legendre functions of the first and second kind, P_ν^μ and Q_ν^μ [19, pp. 1013–1014]:

$$Q_\nu \left(x_1 x_2 - \sqrt{x_1^2 - 1}\sqrt{x_2^2 - 1}\cos\phi \right) = \sum_{k=0}^{\infty} \epsilon_k (-1)^k P_\nu^{-k}(x_1) Q_\nu^k(x_2)\cos(k\phi), \quad (1 < x_1 < x_2),$$

$$P_\nu^{-\mu}(z) = \frac{\Gamma(\nu - \mu + 1)}{\Gamma(\nu + \mu + 1)}\left(P_\nu^\mu(z) - e^{-\mu\pi i}\sin(\mu\pi)Q_\nu^\mu(z) \right). \tag{10}$$

For the half-integer degrees $\nu = n - 1/2$, $n = 0, 1, 2, \ldots$ the associated Legendre functions are commonly called the ring functions, and are the solutions of the Laplace equation in toroidal geometry. They appear, for instance, in Coulomb and gravitational-potential problems [20–22] and in the expansion of a vacuum magnetic field in stellarotors and tokamaks [23]. By separating the singular part of the Green's function and adding a linear combination of the ring functions so that the solution vanishes at the torus $\eta = \eta_0$ we obtain:

$$G_s = \frac{1}{a\pi}\sqrt{(\cosh\eta - \cos\theta)(\cosh\eta' - \cos\theta')}\sum_{m,n=0}^{\infty}\epsilon_m\epsilon_n(-1)^m\frac{\Gamma(n - m + \tfrac{1}{2})}{\Gamma(n + m + \tfrac{1}{2})}\cos[m(\psi - \psi')]\cos[n(\theta - \theta')]$$

$$\times \begin{cases} P_{n-\frac{1}{2}}^m(\cosh\eta)Q_{n-\frac{1}{2}}^m(\cosh\eta') - f(m,\eta,\eta'), & \eta' > \eta, \\ P_{n-\frac{1}{2}}^m(\cosh\eta')Q_{n-\frac{1}{2}}^m(\cosh\eta) - f(m,\eta,\eta'), & \eta' < \eta, \end{cases} \tag{11}$$

where the function f is given by

$$f(m,\eta,\eta') = \frac{P_{n-\frac{1}{2}}^m(\cosh\eta_0)}{Q_{n-\frac{1}{2}}^m(\cosh\eta_0)}Q_{n-\frac{1}{2}}^m(\cosh\eta)Q_{n-\frac{1}{2}}^m(\cosh\eta').$$

By using Eq. 8, the relationship between the unit vectors, $\hat{\psi} = -\sin\psi\,\hat{x} + \cos\psi\,\hat{y}$, and the Fourier series expansion:

$$\delta(\psi - \psi') = \frac{1}{\pi}\sum_{n=0}^{\infty}\epsilon_n\cos[n(\psi - \psi')], \tag{12}$$

we can write:

$$\Delta\tilde{G}\hat{\psi} = -\frac{4\pi}{h_\eta h_\theta h_\psi}\delta(\eta - \eta')\delta(\theta - \theta')\hat{\psi}, \tag{13}$$

where the Green's function $\tilde{G}$ is given by

$$\tilde{G} = -\frac{2}{a}\sqrt{(\cosh\eta - \cos\theta)(\cosh\eta' - \cos\theta')}\sum_{n=0}^{\infty}\epsilon_n\frac{\Gamma(n - \tfrac{1}{2})}{\Gamma(n + \tfrac{3}{2})}\cos[n(\theta - \theta')]$$

$$\times \begin{cases} P_{n-\frac{1}{2}}^1(\cosh\eta)Q_{n-\frac{1}{2}}^1(\cosh\eta') - f(1,\eta,\eta'), & \eta' > \eta, \\ P_{n-\frac{1}{2}}^1(\cosh\eta')Q_{n-\frac{1}{2}}^1(\cosh\eta) - f(1,\eta,\eta'), & \eta' < \eta. \end{cases} \tag{14}$$

By using Eq. 4, with $\tilde{G}$ from Eq. 14, and using the fact that $\mathbf{A}$ and $\tilde{G}$ satisfy the homogeneous Dirichlet boundary condition, we obtain for the vector potential:

$$\mathbf{A} = -\hat{\psi}\frac{\mu_0 I}{2\pi}\sinh\eta_f\sqrt{\frac{\cosh\eta - \cos\theta}{\cosh\eta_f - \cos\theta_f}}\sum_{n=0}^{\infty}\epsilon_n\frac{\Gamma(n - \tfrac{1}{2})}{\Gamma(n + \tfrac{3}{2})}\cos[n(\theta - \theta_f)]$$

$$\times \begin{cases} P_{n-\frac{1}{2}}^1(\cosh\eta_f)Q_{n-\frac{1}{2}}^1(\cosh\eta) - f(1,\eta_f,\eta), & \eta > \eta_f, \\ P_{n-\frac{1}{2}}^1(\cosh\eta)Q_{n-\frac{1}{2}}^1(\cosh\eta_f) - f(1,\eta_f,\eta), & \eta < \eta_f. \end{cases} \tag{15}$$

Since $\sqrt{\cosh \eta_f}\, Q^1_{n-\frac{1}{2}}(\cosh \eta_f) \rightarrow -\pi \delta^0_n/2\sqrt{2}$ for $\eta_f \rightarrow \infty$, we obtain from (15) for the special case of the filament coinciding with the toroidal axis:

$$\mathbf{A} = -\frac{\mu_0 I}{\sqrt{2}} \sqrt{\cosh \eta - \cos \theta} \left[P^1_{-\frac{1}{2}}(\cosh \eta) - Q^1_{-\frac{1}{2}}(\cosh \eta) P^1_{-\frac{1}{2}}(\cosh \eta_0)/Q^1_{-\frac{1}{2}}(\cosh \eta_0) \right] \hat{\psi}. \tag{16}$$

The magnetic field is obtained by substituting the expression for the vector potential in:

$$\mathbf{B} = \nabla \times \mathbf{A} = \frac{1}{h_\theta h_\psi} \frac{\partial}{\partial \theta}(h_\psi A_\psi)\hat{\eta} - \frac{1}{h_\eta h_\psi} \frac{\partial}{\partial \eta}(h_\psi A_\psi)\hat{\theta}. \tag{17}$$

Equation 17 with the vector potential from (15) or (16) and the scale factors from (3) provides an analytic expression for the magnetic field inside the closed superconducting torus, generated by the current filament. An example of the solution is shown in Fig. 3.

We point out that the derived Green's function (14) can be used to solve related vector boundary-value problems of elasticity for a torus, such as the one considered in [24], where instead of Eq. 1 for the magnetic vector potential, a similar equation for the displacement vector has been considered.

We now introduce an infinitesimal cut in the shield, obtained by intersecting the toroidal surface $\eta = \eta_0$ by the half-plane $\psi = \psi_0$ and consider the current distribution on the outside surface of the shield $j_\psi(\eta_0, \theta)$. By employing Eq. 4, we can write for the vector potential at an arbitrary point $(\eta < \eta_0, \theta)$:

$$A_\psi(\eta, \theta) = \frac{\mu_0}{4\pi} \int_{-\pi}^{\pi} d\theta' h_\theta(\eta_0, \theta') h_\psi(\eta_0, \theta') j_\psi(\eta_0, \theta') G^0(\eta, \theta; \eta_0, \theta'), \tag{18}$$

where G^0 is the free-space Green's function obtained from $\tilde{G}$ in (14) by omitting the f term in the curly bracket. Since the toroid is superconducting, it constitutes the magnetic surface, and we can write for the flux through any circle of intersection of the z=const plane and the torus as:

$$LI = \oint \mathbf{A}\mathbf{d}\mathbf{l} = 2\pi r A_\psi, \tag{19}$$

where L is the self-inductance of the torus and $r = r(\eta_0, \theta)$ is the radius of the circle centered at the z-axis. By considering the point on the surface of the toroid in (18) and using (19), we obtain a Fredholm integral equation of the first kind:

$$g(\theta) = \int_{-\pi}^{\pi} d\theta' f(\theta') K(\theta, \theta') \tag{20}$$
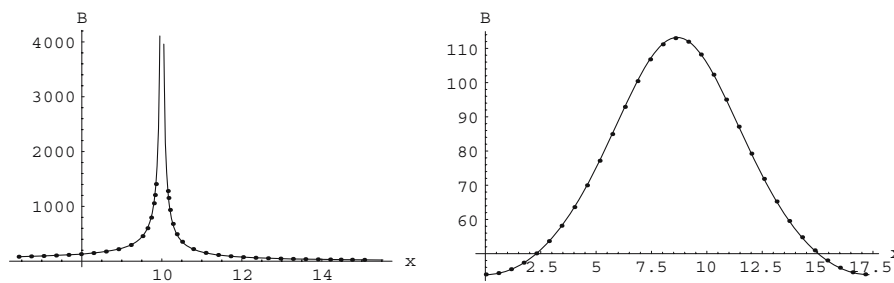
Fig. 3 Magnetic field for the filament located along the toroidal axis of the superconducting torus. The parameters are: $I = 1\,\text{A}$, $a = 10\,\text{mm}$, $\eta_0 = 1\cdot522$. On the left graph, the magnetic field is plotted in the plane of symmetry of the torus; the horizontal axis indicates the radial distance from the z-axis. The ring functions $P^1_{1/2}, Q^1_{1/2}$ have a single branch cut from $-\infty$ to $+1$, and a logarithmic singularity at the location of the filament. On the right graph, the magnetic field is plotted versus the distance along the circle given by the intersection of the torus $\eta = 2$ and a plane containing the z-axis, starting from the point $\eta = 2, \theta = 0$ in the plane. The lines on the graphs show analytic solutions and the solid dots are numerical solutions obtained by a finite-element method. In the numerical approach, the cross-section of the torus is divided into a mesh of triangles and the solution is obtained by minimizing the total energy. At each point within an element, the solution is obtained by a linear interpolation of the values at the three vertices of the triangle. On the graphs, B is given in units of μT and x in mm

for the unknown function:

$$f(\theta') = \frac{j_\psi(\eta_0, \theta')}{(\cosh \eta_0 - \cos \theta')^{3/2} L I}$$

with the symmetrized kernel:

$$K(\theta, \theta') = \frac{G^0(\eta_0, \theta; \eta_0, \theta')}{[(\cosh \eta_0 - \cos \theta)(\cosh \eta_0 - \cos \theta')]^{1/2}},$$

and where the left-hand side is given by

$$g(\theta) = \frac{2}{\mu_0} \frac{\sqrt{\cosh \eta_0 - \cos \theta}}{(a \sinh \eta_0)^3}.$$

We obtain the solution of the above Eq. 20 by a Fourier series expansion:

$$\frac{2}{\mu_0} \frac{1}{r(\eta_0, \theta)} = \sum_k g_k \phi_k(\theta), \quad f(\theta') = \sum_l f_l \phi_l(\theta'), \tag{21}$$

where $\phi(\theta)$ are the eigenfunctions of $K(\theta, \theta')$. We can write the solution in the matrix form:

$$F = K^{-1} G, \tag{22}$$

where F and G are the matrices of coefficients in (21), and K is a diagonal matrix:

$$K_{kl} = \int d\theta \int d\theta' K(\theta, \theta') \phi_k(\theta) \phi_l(\theta'). \tag{23}$$

Using the integral representation of the associated Legendre functions [19, p. 1001]:

$$Q_\nu^\mu(z) = \frac{e^{\mu \pi i} \Gamma(\mu + 1/2)(z^2 - 1)^{\frac{\mu}{2}}}{\sqrt{2}\pi} \left\{ \int_0^\pi dt \frac{t \cos(\nu + 1/2)}{(z - \cos t)^{\mu+1/2}} - \cos \nu \pi \int_0^\infty dt \frac{e^{-(\nu+1/2)t}}{(z + \cosh t)^{\mu+1/2}} \right\}, \tag{24}$$

and relations (10), we can expand the left-hand side in (20) to obtain the coefficients matrix G. Using the fact that the total current is given by $I = \int j_\psi h_\theta d\theta$, we eliminate the self-inductance and finally obtain:

$$j_\psi(\theta) = \frac{I}{a\sqrt{2}} \frac{(\cosh \eta_0 - \cos \theta)^{3/2}}{\Upsilon(\cosh \eta_0)} \sum_{l=0}^\infty \frac{\cos(l\theta)}{(1 + \delta_l^0) P_{l-1/2}^1(\cosh \eta_0)}, \tag{25}$$

where the function Υ is given by

$$\Upsilon(z) = \sum_{l=0}^\infty \frac{2z Q_{l-1/2}(z) - Q_{l-3/2}(z) - Q_{l+1/2}(z)}{(1 + \delta_l^0) P_{l-1/2}^1(z)}. \tag{26}$$

While the current distribution on the inside surface of the toroid, obtained by substituting (15) in (1), is dependent on the location of the filament (being highest at the points closest to the filament and lowest at those diametrically opposite), the distribution given by (25) is independent of the filament location. It is symmetric with respect to the $z = 0$ plane and increases from $\theta = 0$ to $\theta = \pi$ as represented on Fig. 4.

By substituting the expression for the current density (25–26) in (18), we obtain for the vector potential outside the torus:

$$\mathbf{A} = -2\sqrt{2}\mu_0 I \frac{\sinh \eta_0 \sqrt{\cosh \eta - \cos \theta}}{\Upsilon(\cosh \eta_0)}$$

$$\times \sum_{n=0}^\infty \frac{1}{(1 + \delta_n^0)(4n^2 - 1)} \frac{Q_{n-1/2}^1(\cosh \eta_0)}{P_{n-1/2}^1(\cosh \eta_0)} P_{n-1/2}^1(\cosh \eta) \cos(n\theta) \hat{\psi}. \tag{27}$$

The independence of the magnetic field, corresponding to the above vector potential, on the filament location constitutes the ideal behaviour of a CCC. In particular, for two equal-magnitude currents of opposite

direction, at arbitrary locations inside the torus, the magnetic field vanishes everywhere outside the torus. Initially if currents are not of equal magnitude, then, by measuring the magnetic field at any point outside the torus, one can adjust one of the currents until this magnetic field vanishes, which would then ensure that the currents are of equal magnitude. In practice, however, in order to let the current flow on the outside surface, a cut of finite width is introduced. In this case the magnetic field depends on the filament locations, and even when the currents are of equal magnitude, the magnetic field is nonzero. This represents an error in the CCC ratio. We will consider the consequence of the finite cut in the following section.

3 Shield with a thin cut

We now consider the case when the superconducting shield has a radial cut through which the magnetic field "escapes". We introduce the cut as a perturbation in the boundary layer (a general discussion of singular perturbations can be found, for example, in [25, Chap. 3.3]). We are interested in calculating the flux of the magnetic field through the cut as a function of the location of the current filament, the thickness of the shield and the width of the cut. We can represent the currents at the outer surface of the superconductor as $\mathbf{j} = \mathbf{j_0} + \mathbf{j'}$, where $\mathbf{j_0} = j_\psi \hat{\psi}$ is the current distribution (25) in the limit of an infinitesimal cut width, and $\mathbf{j'}$ is the perturbing current distribution due to the finite size of the cut. Since we consider the case of a thin cut, these perturbing currents are located at two narrow symmetrical segments of the torus around the cut. We can approximate these by two strips around the cross-sectional cut of the infinite cylinder and therefore we perform the calculations below in a cylindrical coordinate system.

For subsequent derivations we will need the expressions for the magnetic field, inside and outside the cylinder, far away from the cut. We obtain these by solving Eq. 1 in cylindrical coordinates (ρ, z, ϕ) using the method of the previous section. The current filament, parallel to the z-axis and located at (ρ', ϕ'), is surrounded by a superconducting cylinder of radius ρ_0, with axis coinciding with the z-axis. We obtain for

Fig. 4 Surface-current distribution along the superconducting torus $\eta_0 = 0{\cdot}5, 1, 2$ and 3 (curves further from the origin correspond to higher values of η_0). The graph is a polar plot of $aj_\psi(\alpha)/I$ obtained using (25) with $\theta = \arctan[\sin\alpha \sinh\eta_0/(a + \cos\alpha \cosh\eta_0)]$, where α is the polar angle in the coordinate system with the origin at $a\coth\eta_0, z = 0$, corresponding to the centre of the circle of intersection of a torus and the half-plane $\psi = $const

Polar plot of surface current density
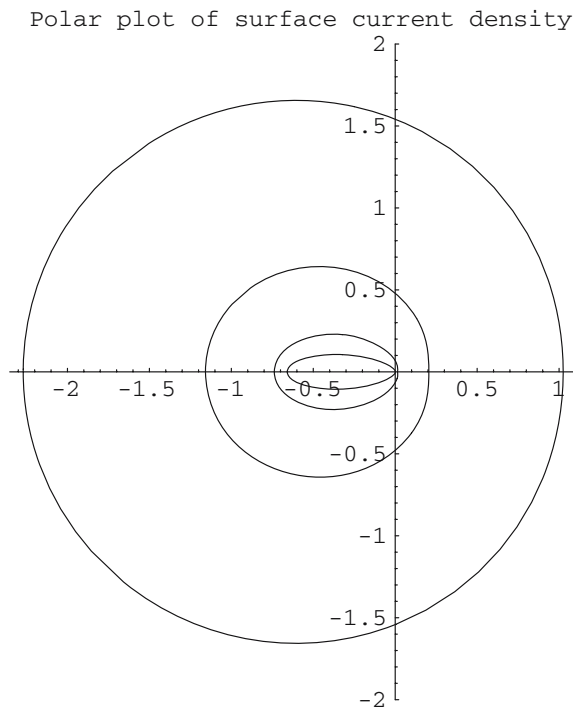
the magnetic vector potential inside the cylinder:

$$\mathbf{A} = -\frac{\mu_0 I}{4\pi} \log \frac{\rho_0^2[\rho'^2 - 2\rho\rho' \cos(\phi - \phi') + \rho^2]}{\rho_0^4 - 2\rho\rho'\rho_0^2 \cos(\phi - \phi') + \rho^2\rho'^2} \hat{\mathbf{z}}. \tag{28}$$

On the outside surface of the cylinder, the current is uniformly distributed so that we have:

$$\mathbf{A} = -\frac{\mu_0 I}{2\pi} \log \frac{\rho}{\rho_0} \hat{\mathbf{z}}. \tag{29}$$

We show in the Appendix, that our approximation is justified in the limit $\eta_0 \gg 1$ where the vector potentials inside the torus, Eq. 15, and outside, Eq. 27, approach the corresponding expressions (28) and (29) in the case of a cylindrical shield.

In the following we will make use of the scalar magnetic potential Φ, defined outside the region with currents as:

$$\mathbf{B} = -\nabla\Phi. \tag{30}$$

Using (28), we obtain inside the cylinder:

$$\Phi = -\frac{\mu_0 I}{2\pi} \arctan \frac{\rho(\rho_0^2 - \rho'^2) \sin(\phi - \phi')}{\rho(\rho_0^2 + \rho'^2) \cos(\phi - \phi') - \rho'(\rho_0^2 + \rho^2)}. \tag{31}$$

For the outside region, we have:

$$\Phi = -\frac{\mu_0 I \phi}{2\pi}. \tag{32}$$

We now introduce a cut in the shield (from $z = -c$ to $z = c$) and are looking for the solution of the Laplace equation:

$$\Delta\Phi = 0 \tag{33}$$

in the form

$$\Phi = \sum_{n=1}^{\infty} \zeta_n(\rho, z) \sin[n(\phi - \phi')], \tag{34}$$

which away from the cut reduces to (31) and (32) inside and outside the cylinder, respectively. Substituting (34) in (33) gives the equation for the Fourier-series coefficients:

$$\frac{\partial^2 \zeta_n}{\partial \rho^2} + \frac{1}{\rho} \frac{\partial \zeta_n}{\partial \rho} + \frac{\partial^2 \zeta_n}{\partial z^2} - \frac{n^2}{\rho^2} \zeta_n = 0. \tag{35}$$

Assuming that $\rho_0 / \max(b, c) \gg 1$, where $2b$ is the thickness of the shield, and introducing the variable $y = \rho - \rho_0$, we can approximate Eq. 35 near the cut by

$$\frac{\partial^2 \zeta_n}{\partial y^2} + \frac{\partial^2 \zeta_n}{\partial z^2} = 0. \tag{36}$$

In order to solve the above equation, we perform the Schwarz-Christoffel mapping (Fig. 5) from $\mathcal{T} = \{t | \Im m\, t > 0\}$ onto the interior of the polygon $w_1, \ldots, w_8$ in the $\mathcal{W}$ plane by

$$\frac{\mathrm{d}w}{\mathrm{d}t} = C \prod_{i=1}^{8} (t - r_i)^{\alpha_i/\pi - 1}, \tag{37}$$

where α_i is the interior angle at the vertex w_i. We let $w_i \to \infty$ for $i = 2, \ldots, 7$, and by the Riemann mapping theorem there are three degrees of freedom in the map, so that we can choose $r_2 = 0, r_5 = \infty$ and $r_8 = -1$. We thus have:

$$w = C \int_{r_1}^{t} \frac{\sqrt{z+1}\sqrt{z-r_1}}{\sqrt{z^3}} \mathrm{d}z + w_1. \tag{38}$$
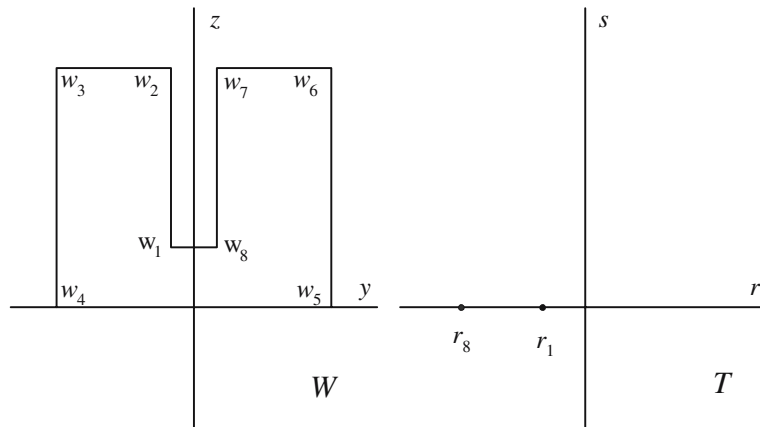
Fig. 5 By the mapping (37), the negative real semi-axis in the $\mathcal{T}$-plane is mapped onto the surface of the superconductor in the $\mathcal{W}$-plane, and the positive real semi-axis in the $\mathcal{T}$-plane is mapped onto the entire real axis in the $\mathcal{W}$-plane. The positive imaginary semi-plane in $\mathcal{T}$ is mapped onto the region outside the superconductor of the positive imaginary part of the $\mathcal{W}$-plane. Using the Schwarz reflection principle, we can continue the mapping (37) analytically into the $s < 0$ half-plane

Considering the points $w = \mathrm{i}c$, and $w = b + \mathrm{i}c$, we have the equation:

$$\int_{r_1}^{r^*} \frac{\sqrt{z+1}\sqrt{z-r_1}}{\sqrt{z^3}} \mathrm{d}z = \int_{r^*}^{-1} \frac{\sqrt{z+1}\sqrt{z-r_1}}{\sqrt{z^3}} \mathrm{d}z, \tag{39}$$

which we solve for r^*. By doing so we obtain that $w = \mathrm{i}c$ corresponds to $r^* = -\sqrt{-r_1}$. By integrating over the semicircle of radius $|r^*|$ in the positive imaginary part of the $\mathcal{T}$-plane (this equipotential is mapped onto the segment $[0, \mathrm{i}c]$ of the imaginary axis in the $\mathcal{W}$-plane) we obtain for the affine constant:

$$C = \frac{c}{2(1 + \sqrt{k})E\left[\frac{4\sqrt{k}}{(1+\sqrt{k})^2}\right]}, \tag{40}$$

where we have denoted the prevertex as $r_1 = -k$. In the above equation, E is the complete elliptic integral of the second kind and k is the solution of the following equation:

$$\frac{\pi}{32} \frac{1-k}{k^{3/2}(1+\sqrt{k})E\left[\frac{4\sqrt{k}}{(1+\sqrt{k})^2}\right]} F\left(\frac{3}{2}, \frac{3}{2}; 3; \frac{k-1}{k}\right) = \frac{b}{c}, \tag{41}$$

where F is the Gauss hypergeometric function. As a function of the ratio b/c, k is represented in Fig. 6.

Fig. 6 Distance from the origin of the prevertex r_1 as a function of the ratio of superconducting wall thickness and cut width
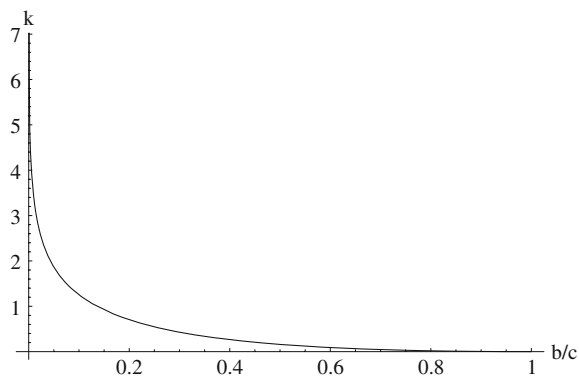
By means of the mapping (38), the function $\zeta_n(y(r,s), z(r,s))$ is a conformal counterpart of the function ξ_n satisfying the two-dimensional Laplace equation in the $\mathcal{T}$-plane with the Neumann boundary condition:

$$\left.\frac{\partial \xi_n}{\partial s}\right|_{s=0} = 0. \tag{42}$$

The harmonic function satisfying the above boundary condition and the symmetry of the problem is given by:

$$\xi_n = \mathsf{P}_n \mathfrak{Re}\left[\log t\right] + \mathsf{Q}_n, \tag{43}$$

where the coefficients P_n and Q_n are determined from the requirement that the potential at the shield surface approaches (31) and (32) inside and outside, respectively, at a distance $p\rho_0$ from the cut, where the parameter $p \sim 1$. In that way we obtain:

$$\xi_n = -\frac{\mu_0 I}{n\pi \log\left[\frac{1}{k}\left(\frac{p\rho_0}{2C}\right)^4\right]} \left(\frac{\rho'}{\rho_0}\right)^n \mathfrak{Re}\left\{\log\left[t\left(\frac{2C}{p\rho_0}\right)^2\right]\right\}, \tag{44}$$

where we have used the fact that, under mapping (38), points $w \sim \pm b + \mathrm{i}(c + p\rho_0)$ on the outer side (upper sign) and the inner side (lower sign) of the shield are the images of the points r_+ and r_-, respectively, and $|r_+| = k/|r_-| \sim (\frac{p\rho_0}{2C})^2$.

Our interest is to obtain the absolute value of the flux of the magnetic field through the cut (B_ρ has the opposite sign of $\sin(\phi - \phi')$). Using the above expression (44) for ξ_n, and Gauss' theorem, we obtain for this flux:

$$\mathcal{F} = \frac{4\mu_0 I \rho_0}{\log\left[\frac{1}{k}\left(\frac{p\rho_0}{2C}\right)^4\right]} \left\{\mathrm{Li}_2\left[\frac{\rho'}{\rho_0}\right] - \frac{1}{4}\mathrm{Li}_2\left[\left(\frac{\rho'}{\rho_0}\right)^2\right]\right\}, \tag{45}$$

where $\mathrm{Li}_2(z) = -\int_0^z \log(1 - z)\mathrm{d}\log(z)$ is the dilogarithm function. The magnetic flux as a function of the superconducting shield thickness, as well as the filament location, are represented in Fig. 7. The inset shows a comparison of the analytical and numerical solution obtained by commercial software. In the numerical approach, a finite-element method was used, with the model being divided into a mesh of tetrahedra. Inside each element, the magnetic field was represented by a polynomial of the fourth degree with unknown coefficients. The finite-element analysis results in the solution of a set of equations for the unknown coefficients.
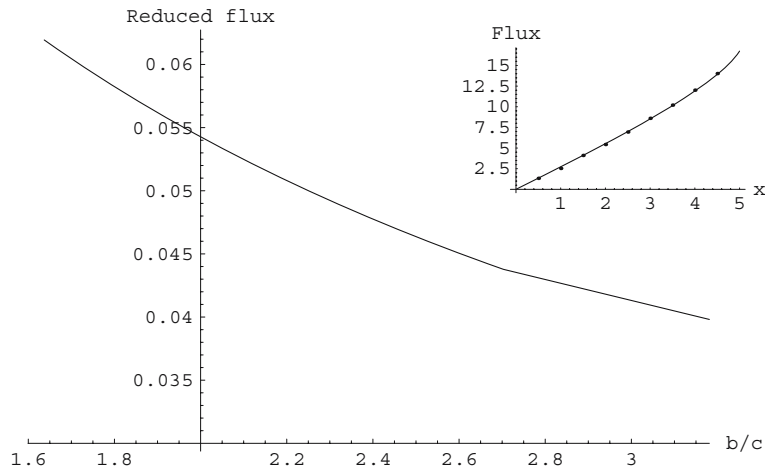
For the general ratio b/c the above Eq. 37 can be integrated explicitly in terms of elliptic integrals, but the inverse function can only be expressed as a Lagrange series. Analytic expressions for the magnetic field away from the gap can be obtained in the limit of negligible shield thickness ($b/c \to 0$). In this case the mapping (37) becomes:

$$w = \frac{c}{2}\left(\sqrt{t} - \frac{1}{\sqrt{t}}\right), \tag{46}$$

which can be used to obtain the derivatives of ζ_n and the potential Φ along the gap in the superconductor ($|z| < c$):

$$\left.\frac{\partial \zeta_n}{\partial \rho}\right|_{\rho=\rho_0} = \frac{\mu_0 I}{2\pi \log\left[\frac{2p\rho_0}{c}\right]} \frac{1}{n}\left(\frac{\rho'}{\rho_0}\right)^n \frac{1}{\sqrt{c^2 - z^2}}, \tag{47}$$

$$\left.\frac{\partial \Phi}{\partial \rho}\right|_{\rho=\rho_0} = \frac{\mu_0 I}{2\pi \log\left[\frac{2p\rho_0}{c}\right]} \tan^{-1}\left[\frac{\rho' \sin(\phi - \phi')}{\rho_0 - \rho' \cos(\phi - \phi')}\right] \frac{1}{\sqrt{c^2 - z^2}}. \tag{48}$$

Fig. 7 Reduced flux $\mathcal{F}' = \mathcal{F}/4\mu_0 I \rho_0 \left\{ \text{Li}_2 \left[\frac{\rho'}{\rho_0} \right] - \frac{1}{4} \text{Li}_2 \left[\left(\frac{\rho'}{\rho_0} \right)^2 \right] \right\}$ as a function of the superconducting shield thickness. The parameters of the shield are as in the experiment in [17]: $\rho_0 = 5$ mm, $b = 1$ mm, and $c = 0.5$ mm. The figure shows that increasing the shield thickness by 50% will decrease the flux by 25%. The inset shows the magnetic flux versus the displacement of the current filament along the x-axis for parameter values: $I = 1$ A, $\rho_0 = 5$ mm, $b = c = 0.5$ mm, $p = 1$. The flux is given in units of 10^{-10} Wb, and the horizontal axis is in mm. The solid lines on the figure are the analytical solution obtained from (45), and solid dots are the numerical solutions. In the numerical approach the height of the cylinder was taken to be $20\rho_0$ and the outer boundary was placed at $2\rho_0$. The edges of the cylinder in the cut cross-section were divided into 1000 segments, the wire was represented by a cylinder of diameter 1 mm and its circumference was divided into 100 sections. The edges in the model, parallel to the superconducting cylinder axis were divided into 30 segments

We solve Eq. 35 by separation of variables, and employing the Fourier-cosine transform along the boundary $\rho = \rho_0$, we obtain:

$$\zeta_n = -\frac{\mu_0 I}{2\pi} \frac{1}{n} \left\{ -\left(\frac{\rho \rho'}{\rho_0^2} \right)^n \Theta(\rho_0 - \rho) + \left(\frac{\rho}{\rho'} \right)^n \Theta(\rho' - \rho) + \left[2(-1)^n - \left(\frac{\rho'}{\rho} \right)^n \Theta(\rho_0 - \rho) \right] \Theta(\rho - \rho') \right.$$

$$\left. + \frac{1}{\log\left(\frac{2p\rho_0}{c} \right)} \left(\frac{\rho'}{\rho_0} \right)^n \int_0^\infty \frac{J_0(c\lambda) \cos(\lambda z)}{\lambda} \left[\frac{I_n(\lambda \rho)}{I_n'(\lambda \rho_0)} \Theta(\rho_0 - \rho) + \frac{K_n(\lambda \rho)}{K_n'(\lambda \rho_0)} \Theta(\rho - \rho_0) \right] d\lambda \right\}, \tag{49}$$

where J_0 is the Bessel function of the first kind, I_n and K_n are the modified Bessel functions of the first and second kind, respectively. Substituting the above expression for ζ_n in Eqs. 34 and 30 gives the explicit solution for the magnetic field. Figure 8 shows the example of the magnetic field in the vicinity of the cut.

In the above derivation, the symmetry of the shield with regard to the z-axis enabled us to find the derivative of the potential along the gap region. For the asymmetric case, with boundary conditions given only for positive z, a Green's functions method was developed for a wave equation in reference [26]. Another example of such an asymmetric case was considered more recently in [27], with solution for the scalar electric potential obtained by using the Wiener–Hopf method.

4 Ratio error

The performance of a CCC is evaluated by considering the ratio error, whereby the magnetic field in the centre of the torus window is sensed by a SQUID in two cases. In one case, two currents of the same magnitude are passed in the opposite directions with filaments placed symmetrically around the axis of the shield. In the other case the current flows through one of the filaments only. The CCC ratio error is then given by the ratio of the magnetic field detected in each case.
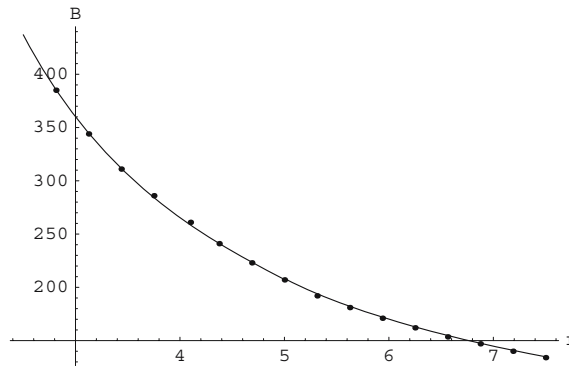
Fig. 8 Magnetic field versus the distance from the z-axis for the parameters: $I = 5\,\text{A}$, $\rho_0 = 5\,\text{mm}$, $\rho' = c = 0.5\,\text{mm}$, $z = 4\,\text{mm}$, $\phi = \pi/3$ and $p = 1.5$. The solid line on the graph is the analytic solution obtained from formulas (30), (34) and (49). The solid dots show the numerical solution obtained by solving Maxwell's equations using the finite-element method with the boundary condition of zero normal component of the magnetic field on the surface of the superconductor. The height of the cylinder was 100 mm. B is expressed in μT and r in mm

Following the procedure of Sect. 3 to derive ζ_n, for the case of two filaments located at $(\rho = \rho', \phi = 0)$ and $(\rho = \rho', \phi = \pi)$ through which equal amplitude currents flow in opposite directions and using the expression for the magnetic field of the loop of radius a in free space, we obtain for the ratio error r of the CCC, in the lowest order of ρ'/ρ_0:

$$r = \frac{4}{\pi} \frac{1}{\log\left(\frac{2p\rho_0}{c}\right)} \frac{\rho'}{\rho_0} \int_0^\infty \frac{J_0(xc/a)K_1(x)}{x\left[K_0(x\rho_0/a) + K_2(x\rho_0/a)\right]} \, \mathrm{d}x. \tag{50}$$

Using the asymptotic behaviour of Bessel functions for small arguments $0 < x \ll \sqrt{\alpha + 1}$:

$$J_\alpha \to \frac{1}{\Gamma(\alpha+1)}\left(\frac{x}{2}\right)^\alpha, \quad K_\alpha \to \begin{cases} -\log(x/2) - \gamma, & \alpha = 0, \\ \frac{\Gamma(\alpha)}{2}\left(\frac{2}{\alpha}\right)^\alpha, & \alpha > 0, \end{cases}$$

we approximate the kernel in (50) by the Lorentzian $\frac{1}{2}\left(\frac{\rho_0}{a}\right)^2 \frac{1}{1+x^2}$ and obtain a simplified expression for the ratio error:

$$r = \frac{1}{\log\left(\frac{2p\rho_0}{c}\right)} \frac{\rho'\rho_0}{a^2}. \tag{51}$$

There is little experimental evidence available at this stage to compare with the theoretical result, but by substituting the values for the parameters from [17]: $\rho' = 1.5\,\text{mm}$, $\rho_0 = 5\,\text{mm}$, $a = 15\,\text{mm}$, $c = 0.5\,\text{mm}$, and taking $p = 1$, we obtain for the ratio error $r \sim 1\%$, which is consistent with experiment.

The above formula shows that the easiest way to decrease this value in practice is by increasing the radius a and concentrating the currents near the axis. The dependence of the error on cut thickness is logarithmic; therefore, to reduce the error for example by a factor of 3 would require decreasing the cut thickness to μm size. This is difficult but perhaps could be done by oxidizing the superconducting surface over the cut area and clamping the shield.

5 Concluding remarks

We have considered the magnetic field of an HTS CCC. We have first considered the case of a toroidal superconducting shield with an infinitesimal radial cut and obtained the expression for the magnetic vector potential. By solving the Fredholm integral equation we have obtained an analytic expression for the

current distribution on the outer surface. These findings will be useful for the sensitivity analysis of an HTS CCC similar to those developed for a low-temperature superconducting CCC [12, 13].

In order to obtain the leakage flux of the magnetic field we have neglected the curvature of the torus; that is, we have approximated the shield to be of a cylindrical shape. We have found the solution for the magnetic scalar potential in the form of a Fourier-sine series which approaches the asymptotic expression far away from the cut. In order to obtain the coefficients in this expansion, we have conformally mapped the region of interest (the area outside the superconductor) in the azimuthal plane onto the positive imaginary part of another complex plane. In this way, we have obtained the leakage flux through the cut as well as an explicit expression for the magnetic field (in the limit of vanishing superconductor thickness). The analytic results are in good agreement with numerical results obtained by a finite-element method. By extending the consideration to include another filament inside the shield, we have obtained an expression for the ratio error measured at the centre of the toroid. For the measurement of the field flux through a pickup coil located at the torus window, this ratio can be obtained by integrating the flux through the half-plane outside the cylindrical shield, using expression (34) with coefficients given by (49), and using expression (27) for the toroidal shield.

The ratio error formula (51) shows that the error decreases by increasing the toroidal radius, and decreasing the inner radius of the shield. According to the formula, the filaments should be centered around the axis to minimize the error. The leakage flux (45) decreases with increasing the material thickness. The cut width enters the ratio error only logarithmically, so considerable effort in its reduction is needed for observable improvement. For the best performance, the superconducting shield can be surface treated over the area of the cut, with the insulating layer being of the order of a micron, which would be thick enough to prevent the tunneling current across the gap. In that case formula (51) shows that, in combination with reducing the bore radius by a factor of three, the ratio error would be reduced by an order of magnitude, for the same filament location and toroid radius.

Of interest for further study is the extension of the present work to several concentric superconducting toroidal shields which reduce the ratio error by screening the cut, and a study of the performance of an HTS CCC in the case of ac rather than dc currents.

Appendix

In this appendix we show that for $\eta_0 \gg 1$ we can map the boundary-value problem from a toroidal to a cylindrical geometry. By using the transformation [28, p. 336]:

$$P^{\mu}_{\nu-\frac{1}{2}}(\cosh \eta) = \frac{2^{2\mu}}{\Gamma(1-\mu)(1-e^{-2\nu})^{\mu}e^{(\nu+\frac{1}{2})\nu}}F\left(\frac{1}{2}-\mu, \frac{1}{2}+\nu-\mu; 1-2\mu; 1-e^{-2\nu}\right), \tag{52}$$

and expanding the hypergeometric function $F(a, b; a+b; z)$ around $z \to 1$, we have:

$$P^{1}_{-\frac{1}{2}}(\cosh \eta) \approx -\frac{1}{\sqrt{2}\pi}\frac{\log(2\cosh \eta) - \gamma - \psi(-\frac{1}{2})}{\sqrt{\cosh \eta}}, \tag{53}$$

where $\psi(z) = \Gamma'(z)/\Gamma(z)$ is the digamma function. By using [28, p. 336]:

$$Q^{\mu}_{\nu-\frac{1}{2}}(\cosh \nu) = \frac{\sqrt{\pi}e^{i\mu\pi}\Gamma(\frac{1}{2}+\nu+\mu)(1-e^{-2\eta})^{\mu}}{\Gamma(1+\nu)e^{(\nu+\frac{1}{2})\eta}}F\left(\frac{1}{2}+\mu, \frac{1}{2}+\nu+\mu; 1+\nu; e^{-2\eta}\right), \tag{54}$$

and expanding $F(a, b; c; z)$ around $z \to 0$, we can write:

$$Q^{1}_{-\frac{1}{2}}(\cosh \eta) \approx -\frac{\pi}{2\sqrt{2}}\frac{1}{\sqrt{\cosh \eta}}. \tag{55}$$

By introducing the distance from the axis $\rho = [(\sqrt{x^2 + y^2} - a)^2 + z^2]^{1/2}$, and considering the inverse transformations of (2), we obtain $\cosh \eta \approx a/\rho$. Substituting this in (53) and (55) we get for the $n = 0$ term in (15):

$$-\frac{\mu_0 I}{2\pi}\left[\Theta(\rho' - \rho)\log\frac{\rho'}{\rho_0} + \Theta(\rho - \rho')\log\frac{\rho}{\rho_0}\right]. \tag{56}$$

For the terms $n \geq 1$ in (15) we use (52) and (54) and the expansions of $F(a, b; a + b - n; z)$ around $z \to 1$ for $P^1_{n-\frac{1}{2}}$ and the expansion of $F(a, b; c; z)$ around $z \to 0$ for $Q^1_{n-\frac{1}{2}}$ to obtain:

$$\begin{aligned}
P^1_{n-\frac{1}{2}}(\cosh \eta) &\approx \frac{2^n}{\sqrt{2\pi}}\frac{\Gamma(n)}{\Gamma(n-\frac{1}{2})}(\cosh \eta)^{n-\frac{1}{2}}, \\
Q^1_{n-\frac{1}{2}}(\cosh \eta) &\approx -\frac{\sqrt{\pi}}{2^{n+\frac{1}{2}}}\frac{\Gamma(n+\frac{3}{2})}{\Gamma(n+1)}\frac{1}{(\cosh \eta)^{n+\frac{1}{2}}}.
\end{aligned} \tag{57}$$

By substituting (57) in (15) we get the following expression:

$$-\frac{\mu_0 I}{2\pi}\frac{1}{n}\left\{\Theta(\rho' - \rho)\left(\frac{\rho}{\rho_0}\right)^n\left[\left(\frac{\rho'}{\rho_0}\right)^n - \left(\frac{\rho_0}{\rho_0'}\right)^n\right] + \Theta(\rho' - \rho)\left(\frac{\rho}{\rho_0}\right)^n\left[\left(\frac{\rho'}{\rho_0}\right)^n - \left(\frac{\rho_0}{\rho_0'}\right)^n\right]\right\}. \tag{58}$$

By combining (56) and (58) we arrive at (28). By substituting (53), (55) and (57) in (27) we obtain (16), which close to the shield $\eta \lesssim \eta_0$ reduces to (29). In that way, the potentials away from the cut on the torus in this approximation approach the expressions for the cylindrical shield.

References

1. Witt TJ (1998) Electrical resistance standards and the quantum Hall effect. Rev Sci Instrum 69:2823–2843
2. Feltin N, Devoille L, Piquemal F, Lotkhov SV, Zorin AB (2003) Progress in measurements of a single-electron pump by means of a CCC. IEEE Trans Instrum Meas 52:599–603
3. Rietveld G, Bartolomé E, Sesé J, de la Court P, Flokstra J, Rillo C, Camón A (2003) 1:30000 Cryogenic current comparator with optimum SQUID readout. IEEE Trans Instrum Meas 52:621–625
4. Williams JM, Kleinschmidt P (1999) A cryogenic current comparator bridge for resistance measurements at currents of up to 100 A. IEEE Trans Instrum Meas 48:375–378
5. Seppä H, Satrapinski A, Kiviranta M, Virkki V (1999) Thin-film cryogenic current comparator. IEEE Trans Instrum Meas 48:365–369
6. Piquemal F, Genevés G (2000) Argument for a direct realization of the quantum metrological triangle. Metrologia 37:207–211
7. Lotkhov SV, Bogoslovsky SA, Zorin AB, Niemeyer J (2001) Operation of a three-junction single-electron pump with on-chip resistors. Appl Phys Lett 78:946–948
8. Bubanja V (2002) Influence of the electromagnetic environment on the accuracy of the single electron pump. J Phys Soc Jpn 71:1501–1505
9. Keller MW, Eichenberger AL, Martinis JM, Zimmerman NM (1999) A capacitance standard based on counting electrons. Science 285:1706–1709
10. Mohr PJ, Taylor BN (2000) CODATA recommended values of the fundamental physical constants: 1998. Rev Mod Phys 72:351–495
11. Seppä H (1990) The ratio error of the overlapped-tube cryogenic current comparator. IEEE Trans Instrum Meas 39:689–697
12. Early MD, Jones K (1999) Optimum sensitivity of an externally shielded cryogenic current comparator. IEEE Trans Instrum Meas 46:459–463
13. Sesé J, Rietveld G, Camón A, Rillo C, Vargas L, Christian G, Brons S, Hiddink MGH, Flokstra J, Rogalla H, Jaszczuk W, Altenburg H (1999) Design and realisation of an optimal current sensitive CCC. IEEE Trans Instrum Meas 48:370–374
14. Hao L, Gallop JC, Macfarlane JC, Carr C (2003) HTS cryogenic current comparator for non-invasive sensing of charged particle beams. IEEE Trans Instrum Meas 52:617–620
15. Elmquist RE (1999) Cryogenic current comparator measurements at 77 K using thallium-2233 thick-film shields. IEEE Trans Instrum Meas 48:383–386
16. Early MD, Jones K, van Dam MA (2000) Development of an HTS cryogenic current comparator. In: Obradors X, Sandiumenge F, Fontcuberta J (eds) Applied supperconductivity 1999. Institute of Physics Publishing, Bristol pp 517–520

17. Early MD, Jones K, Staines MP, Exley RR (2001) Development of a split-toroid high-temperature superconducting cryogenic current comparator. IEEE Trans Instrum Meas 50:306–309
18. Morse PM, Feshbach H (1953) Methods of theoretical physics. McGraw-Hill, New York
19. Gradshteyn IS, Ryzhik IM (1994) Table of integrals, series, and products. Academic Press, New York
20. Cohl HS, Rau ARP, Tohline JE, Browne DA, Cazes JE, Barnes EI (2001) Useful alternative to the multiple expansion of 1/r potentials. Phys Rev A 64:052509
21. Cohl HS, Tohline JE (1999) A compact cylindrical Green's function expansion for the solution of potential problems. Astrophys J 527:86–101
22. Cohl HS, Tohline JE, Rau ARP, Srivastava HM (2000) Developments in determining the gravitational potential using toroidal functions. Astron Nachr 321:363–372
23. van Milligen BPh, Lopez Fraguas A (1994) Expansion of vacuum magnetic fields in toroidal harmonics. Comput Phys Commun 81:74–90
24. Krokhmal PA (2002) Exact solution of the displacement boundary-value problem of elasticity for a torus. *J. Engng. Math.* 44:345–368
25. Kevorkian J, Dole JD (1996) Multiple scale and singular perturbation methods. Springer-Verlag, New York
26. Levine H, Schwinger J (1948) On the radiation of sound from an unflanged circular pipe. Phys Rev 73:383–406
27. Ursescu A, Eckart W, Marschall H, Hutter K (2004) Inhomogeneous electric field generated by two long electrodes placed along infinite walls separating different dielectric media. J Engng Math 49:57–75
28. Abramowitz M, Stegun IA (1972) Hanbook of mathematical functions. Dover Publications, Inc. New York